Mapping Paddy Growth Stage Based-on Hyperspectral EO-1 Hyperion using Pixel Purity Index Endmember Extraction Algorithm

Hertanto Suryoprayogo, Fatwa Ramdani, Fitri Utaminingrum
Faculty of Computer Science, Brawijaya University, Malang, 65145, Indonesia.
hertanto.suryoprayogo@gmail.com

***Abstract*—Hyperspectral remote sensing is widely used in monitoring vegetation because it provides a high spatial and spectral resolution. Thus, its ability to distinguish between various objects on earth. However, many problems arise in processing Hyperspectral data. In this paper, Pixel Purity Index algorithm is used in addressing this issue. PPI is an endmember extraction method which is widely used in hyperspectral data processing because it can handle mixed pixel on large resolution images as well as reduce the dimensionality of the data. In vegetation mapping, determining the wavelength plays an important role in object reflectance analysis. In this study, paddy reflectance characteristics are examined, where results show that the characteristics of paddy occur in wavelength 447, 701, 1024, and 1104 nm. In the region of VIS-red edge (447-701nm), curve below value of 0.1 can be used to distinguish among paddy and non-paddy vegetation reflectance, while the combination of the increase/decrease value in red edge-NIR (701-1027nm) and NIR-SWIR (1027-1104nm) range, can be used as a reference for analyzing the reflectance of rice growth, wherein the mean value of red edge-NIR can be used as predictors in distinguishing the paddy growth stage**.

***Index Terms*—Endmember Extraction; Hyperspectral; Paddy; Pixel Purity Index.**

I. INTRODUCTION

Rice (*Oryza sativa L.*) is a majority staple food [1] in Asian countries, including Indonesia [2]. More than 200 varieties of rice in Indonesia has been discovered since 1930, with various advantages and characteristics [3]. However, the conventional methods of monitoring paddy field through ground surveys and interviews with farmers will be time-consuming [4], also destroying the crop field [5]. Thus, usage of digital technologies in resulting a non-destructive and detailed measurements in mapping [5] which effective in observation time is needed as a solution in managing agricultural resources, as well as improve the precision assessment [1]

One of the most methods in natural resource monitoring and assessment digital technologies can be done through remote sensing [6]. In remote sensing technology, Hyperspectral sensor is widely used in processing information because of its ability in provides an accurate and detailed prediction for crop yields, distinguish vegetation varieties [9] biochemical content estimation as well as the absorption features from various object on earth [2], which cannot provided by multispectral sensors [2][4]. One of the hyperspectral sensor systems is produced by Earth Observer 1 (EO-1) Hyperion Imagery, which applied the concept of high spectral, spatial and radiometric resolution [8] that separated the features in the observation area into a region, through the electromagnetic spectrum recorded in the spectral library, provides detailed mapping and classification result [7] as well as identify various spectral objects [8].

However, some problems generally arise in Hyperspectral data processing. The data dimensions will also increase along with the increase in Hyperspectral spectral resolution. This leads to some limitations in computing and data processing [10]. In addition, the digital image often contains noise [11], and will not representative for processing. Besides, each pixel of the digital image will bring up issues or pixel mixture. Whereas for classification, a training sample must have a clear representation in class property [10]. According to Mozaffar et al. [12], a mixed pixel image is an element that represents an area and which includes more than one type of cover. In remote sensing, the endmember selection is an essential part in resulting good mapping into sub fraction image [13]. One of the critical issues with hyperspectral image processing is the breakdown of a mixed pixel into sub-pixel and fraction endmember spectral signatures through spectral unmixing. Spectral unmixing is a method for endmember extraction that is carried out in hyperspectral data processing to choose the pure endmember signatures for a class [14] or pure pixels that contribute to the mixture [8] using a signature matrix to find endmember in the image [15].

A method of overcoming this problem is required to perform dimension reduction in the dataset by removing the band with the high value of noise and replacing with the band which has optimal information for further processing of the data, as well as methods of selecting endmember features of the smallest subset in order to minimize redundant information, provide fast computing and perform spectral unmixing in mixed pixels of the image. In the last few years, many methods were developed to reduce the dimensions of the data and for extracting endmember. According to Chaudhry, et al. [15] in previous research, some algorithm was developed to find endmember in the image data, including the Pixel Purity Index (PPI), N-finder (N-FINDR) algorithm, Iterative Error Analysis (IEA), Automated morphological Endmember Extraction (AMEE) algorithm, Minimum Volume Transform, Convex Geometry, and so on. However, PPI is more widely used [13] because of its ability to extract endmember and its availability in the ENVI software package [15][20]. In addition, the Minimum Noise Fraction (MNF) method in PPI is widely used in reducing the dimensionality of the hyperspectral data by eliminating bands with high noise values, and vegetation mapping [21].

In remote sensing, the reflectance value of an object is

represented by a curve or graph known as a spectral signature. Spectral library has unique characteristics as a reference for the study of various biomass content of vegetation where the value can be observed at each wavelength range, such as the value of photosynthetic pigments (400-700 nm) and chlorophyll absorption (600 nm) in the early range spectra, red edge-chlorophyll (700-750 nm) on the second range spectra, liquid water variation (1080-1170 nm) in the third region spectra, variations in leaf waxes and oil (1700-1780 nm) and cellulose (2100 nm) in the fourth region spectra, the amount of soil (2100-2300 nm) and nitrogen/protein (2280-2290 nm) [16]. One common method used to calculate chlorophyll and leaf canopy is an area index (LAI, leaf area per unit ground area), which is used as an indicator of the status of paddy, based on the phase of growth [17]. Hyperspectral remote sensing is widely used as a method of getting information about vegetation crop based on LAI in the canopy [17-21], [27-28] that can measure the value of reflectance in a variety of continuous narrow spectral bands. Thenkabail et al [18] recommended 12 narrow bands which provide optimum crop information in the range of 350-1050nm, while 400-2500nm narrowband was for the broader range. A total of 22 bands is optimally used to characterize vegetation and agricultural crops [19].

More specifically, many previous research on paddy reflectance measurement were conducted. These study focuses on the development and selection of spectral reflectance signature of paddy and discusses the method of identifying paddy reflectance profile [1], which can be used to distinguish varieties [2], growth stage [29], panicle [6], biomass [5], by using hyperspectral data [4][16][22-26]. Furthermore, the paddy spectral reflectance signature will be used as a reference in the spectral library. Wavebands 444, 594, and 1510 nm are useful in monitoring vegetation based on LAI value [23]. In addition, Red edge and NIR regions of the spectra play an important role in discrimination on the crop species [21][28]. While in paddy field monitoring research, Wang [23] reported having 15 optimal wavebands in 9 phases of paddy growth stage in the range of 350-2500 nm. Where the frequency of the highest wavelength value occurs at 554, 675, 723, and 1633 nm, also 444, 524, 576, 594, 804, 849, 974, 1.074, 1.219, 1.510, and 2194 nm. These waveband values are used as indicators for unique paddy rice spectral signature and investigated to measure the value of LAI using remote sensing data. Moharana, et al [26] identified wavebands rice canopy spectral signatures that are sensitive to nitrogen content within the ranges of 350-1050 nm as the basis for classification in distinguishing between rice varieties. Where the results of these studies show the spectral wavebands significant in distinguishing paddy are 519.559 nm in Green region which shows the absorption of chlorophyll, 649 nm in Red region, and 729 nm in the Red edge which is centered in the range of 700-720 nm [27]. High reflectance value in the green region and transition between red and NIR reflectance (red edge) which varies between 680-710 nm, NIR (779.819 nm), and 779.819 nm has the reflectance characteristics that can be used to distinguish between rice genotypes, because of its sensitivity to nitrogen content. According to Song [22], the narrowband that is most sensitive to nitrogen content and is useful for distinguishing between rice leaves is 552, 675, 705 and 776 nm, in addition to narrowband SWIR in 1158, 1378 and 1965 nm which is useful in distinguishing the spectra of rice under irrigation conditions. According to Kuenzer [25], the characteristics of rice becomes visible and will appear on NIR (red edge) within the value of chlorophyll in the leaves, of which the radiation absorption process is strongly influenced by leaf pigments. Shwetang et al. [16], recommended the selected wavelengths based on the characteristic value of reflectance spectra of paddy that has increased in the range of 33-96 (681-1104 nm), 102-163 (1164-1780 nm), 183-184 (1981-1991 nm), 187-220 (2022-2355 nm). Where the value of reflectance spectra decreases, and has a negative value and it is zero in bands 8-32 (426.82-671 nm), 97-101 (1114-1154 nm), 164 (1790 nm), and 185-186 (2002-2012 nm). According to Chang et al. [24], the characteristics of reflectance of rice during the early 3 weeks planting is influenced by the soil and water. While in phases 6 and 9 weeks, the worth of leaf area will increase, and at week 12, values of reflectance in the NIR region will attain its maximum value and its minimum value is attained in the visible region.

The objective of this study is to determine the paddy endmember based on EO-1 Hyperion imagery using the Pixel Purity Index (PPI) endmember extraction algorithm, by selecting the most meaningful and unique wavelength in describing LAI and optimum nitrogen content information for distinguishing between paddy growth stage spectral signatures based on the wavelength selection of literature study.

II. Material and Methods

A. Data and Study Area

The location of research is Pasuruan, East Java, Indonesia, with a geographical location between 7°40'31.86"-7°45'1.28"S and 112° 51'55.70"-112°55'43.88"E with majority land use of residential and paddy field (Figure 1). Satellite imagery data used in this study is EO-1 Hyperion Hyperspectral L1Gst. EO-1 Hyperion has 242 bands in Band Sequential (BSQ) format, consisting of 70 Visible-Near Infrared (VNIR/VIR+NIR) bands in 400-1000 nm spectral range with a full-width at half maximum (FWHM) of 10.90 and 172 shortwave-infrared (SWIR) bands in 900-2500 nm spectral range with an FWHM of 10.14nm. and 172 shortwave-infrared (SWIR) bands in 900-2500 nm spectral range with an FWHM of 10.14nm.

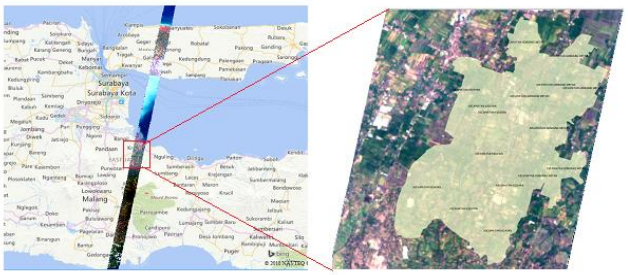

Figure 1: Location of Study area in Pasuruan, East Java, Indonesia.

B. Methodology

The research methodology was performed using the Hyperspectral band statistical analysis, to observe the band with optimal value for the subsequent process of the spatial and spectral subset. The next step in Hyperion image pre-processing is conducted through radiometric calibration and Atmospheric correction. The TOA reflectance image will be used as input in the MNF which aims to eliminate noise in the image. Furthermore, the process for endmember image extraction is through the PPI and the n-D visualizers. After

these endmembers were extracted, further analysis is performed to distinguish paddy endmember, based on the growth stage. Furthermore, the mapping is done through unmixing method to search for pure endmember rice planting season through the SAM based on the reflectance image input. The research methodology is illustrated in Figure 2.

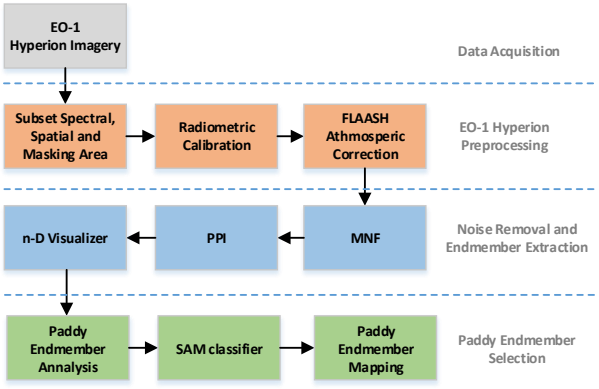

Figure 2: Research Methodology

C. EO-1 Hyperion Pre-processing

Hyperspectral data processing is required in the initial analysis of the spectral statistical data. Spectral analysis is useful in selecting a band that has the optimum value to be used in subsequent image processing. In the spectral subset process, the bands which do not have the information (bad bands) are identified and eliminated. The analysis is done by observing the statistics spectral band, where the hyperspectral band generally do not have a calibration value in band 1-7, 58-76, and 225-242 [30]. Furthermore, there are a number of zero value (non-calibrated) bands in 50, 52, 54, 56, 77, 79, 81, 83, 85, 87, 89, and 91. Besides, the number of bands in the 121-126, 167-180, 222-224 has overlap region value and vapor water absorption [31]. These bad band list which consist of bands: 1-7, 50, 52, 54, 56, 58-77, 79, 81, 83, 85, 87, 89, 91, 121-126, 167-180, and 222-242 will be eliminated. The spectral subset is conducted using 163 spectral bands with optimal information (Table 1).

Table 1
EO-1 Hyperion Calibrated Band used in the Study

Region		Band	Wavelength (nm)	Total
VNIR	VIR	8-31	426.82 - 660.85	24
	NIR	32-49, 51, 53, 55, 57	671.02 - 864.35	22
SWIR 1		78, 79, 81, 83, 85, 87, 89, 91, 92-120	1027.16 - 1346.25	36
SWIR 2		127-166	1416.94 - 1810.38	40
SWIR 3		181-221	1961.66 - 2365.2	41

Once the data have selected by using only data with meaningful information, the next step is pre-processing data by radiometric calibration and atmospheric correction. Radiometric calibration is performed on an image which is spatially subsetted by administrative boundaries and spectrally subset using 163 spectral bands. In the spectral statistical properties of the image, Radiance Gains value in VNIR is 0.025, while in the SWIR is 0.0125. Radiometric calibration will convert the value of Digital Number on the VNIR and SWIR band into radiance value in units of W/m^2 sr µm, by dividing the VNIR DN value into LRadiance with 40 (DN / 40) and dividing the SWIR DN value into LRadiance by 80 (DN / 80) [16]. Hyperion radiance is calibrated by converting BSQ (Band Sequential) format into the BIL (Band Interleave) format using a scale factor of 0.1.

To obtain spectral information from satellite imagery, the reflectance value of the object is necessary. The reflectance value is obtained from the TOA (Top of Atmosphere) value. The next step in pre-processing is the atmospheric correction to convert the DN Radiance value into a reluctance TOA (Top of Atmosphere) value using FLAASH module. FLAASH is used to reduce the atmospheric effects on the reflectance of the object [16]. Results showed that the average visibility is 10.86 km and water content was 0.69 cm. Furthermore, the reflectance value is scaled into reflectance value of 0-1.

D. Minimum Noise Fraction (MNF)

MNF is used to reduce the computing process through segregate dimensionality of the data by determining the inherent noise [32]. MNF is conducted through two Principal Component (PC) transformations, wherein the first transformation will separate and rescale noise in the data based on the noise covariance matrix, which the second transformation is the noise whitened data [33][34]. The data dimensionality is determined by eigenvalues selection in the images which divided the data space into two parts. The first part will be associated with a large eigenvalue and coherent eigenimages, and the second part will be associated with a near value to large eigenvalues which are dominated by noise. By using coherent portion, the noise will be separated from the data, thus improve the spectral processing results. Eigenvalues and eigenimages were used to evaluate the dimensionality of the data. Eigenvalues are sorted from the larger value into a smaller value that only contains noise. The image resulted through MNF will be spatially coherent, wherein the image which contain noise will not have spatial information [34].

E. Pixel Purity Index (PPI)

Pixel Purity Index (PPI) is an algorithm developed by Research System Software Package, Environment for Visualizing Images (ENVI). In Hyperspectral analysis, PPI is used to determine the potential endmember spectra of images through spectral unmixing, whereby in the n-Dimensional spectra space, the endmember spectra will be along the margin of the cloud data [34]. The purpose of PPI is to find pixel which has the purest spectral value and spatial information or the location of each pixel represents pure endmember. PPI will compute random vector unit repeatedly by projecting the random vector in the n-D scatter plots. The extreme pixel which is farthest from the unit vector in each projection will be recorded, also the number of occurrences of the pixel will be marked as extreme. An image output PPI will be generated such that each pixel value corresponds to the number of times the pixels are recorded as extreme. In calculating PPI, the PPI high value means a pixel image is recorded as endmember on many iterations [33][36-37].

F. n-D Visualizer

n-dimensional visualizer is an interactive tool used to determine the location, identification, and spectral cluster, that is, the purest or unique pixel in the image, and visualize pixel selected through the PPI scatter plot [33][38-39].

G. Spectral Angle Mapper

SAM is one of the methods used in addressing the pure endmember. This is achieved through unmixing in the mixed pixel. In this study, spectral unmixing is conducted using SAM to measure the pure spectral value of the object with the input spectral library of endmember. Through SAM, individual spectra represented as a vector in space dimensionality will be compared, and the similarity between two spectra is determined by calculating the angle between them. Spectral mixing using SAM provides mapping by the calculation of the dominant material contained in pixel [33-34].

H. Paddy Reflectance

Endmember generated through the PPI will be stored in a spectral library and analyzed based on the wavelength value in the reflectance curve of the object. In this study, the paddy reflectance will be grouped based on the paddy reflectance characteristics from previous research. Whereas, the VNIR, Red edge and NIR region have an important role to play in distinguishing between crop species. The value of the VNIR will be high in the early phase of planting and will decrease after a phase of 12 weeks. Where the leaf area value will be high in the initial phase of planting and reach the peak at a 12-week phase but decrease after 12-15 week phase. Selection of wavelength is summarized in Table 2. In the initial analysis of vegetation, the VIS value below 0.1 will be classified as non-vegetation and vegetation of non-paddy. Furthermore, the characteristic curve is distinguished by three categories mean value curve on VIS (447-701 nm), red edge-NIR (701-1027 nm) and NIR-SWIR (1027-1104 nm). Analysis is performed on the increase/decrease value as well as value mean in the red edge-NIR, and increase/decrease value in the NIR-SWIR.

Table 2
Paddy Wavelength Selection (nm) based on Literature

Range		Wang [23]	Moharana [26]	Song [22]	Shwetank [16], Kumar [2]	This study
VNIR (440-1000 nm)	VIS (440-730 nm)	554 675 723	519 559 649	552 675 705		447-701 (VIS-red edge)
	NIR (730-1000 nm)		729 779	776	681.20 - 1104.19	701- 1027 (red edge-NIR)
SWIR (1000-2400 nm)		1633			1164.68 - 1780.09 1981.86-1991.96	1027-1104 (NIR- SWIR)

III. Result

Reflectance Image (Figure 3c) used as input in MNF process. MNF is a general reduction method used for selecting the spectral bands that have optimal information by removing bands with high noise. In determining the dimensionality of the band, a spatial coherence value method was used with a threshold value on MNF eigenvalue. The threshold value of 2 was used in this process, because the value close to 1 will have high noise. Where there are 53 MNF bands that have a value higher than 2 used as a new image with smaller dimensionality by removing bands that do not have optimal information or noise. However, it still bears the value of the entire band information. Eigenvalue in MNF Iteration and the process of determining spatial dimensionality through Spatial Coherence Value is shown in Figure 3a and 3b, while the composite MNF Eigenimages output is shown in Figure 4b.

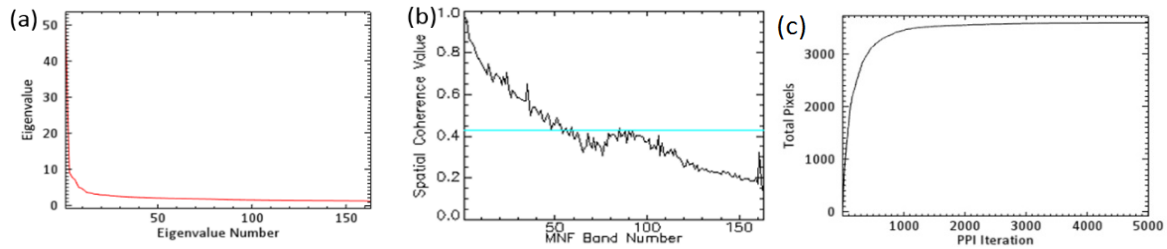

Figure 3: Eigenvalue in (a) MNF iteration; (b) spatial dimensionality determination through Spatial Coherence Value; (c) PPI Iteration.

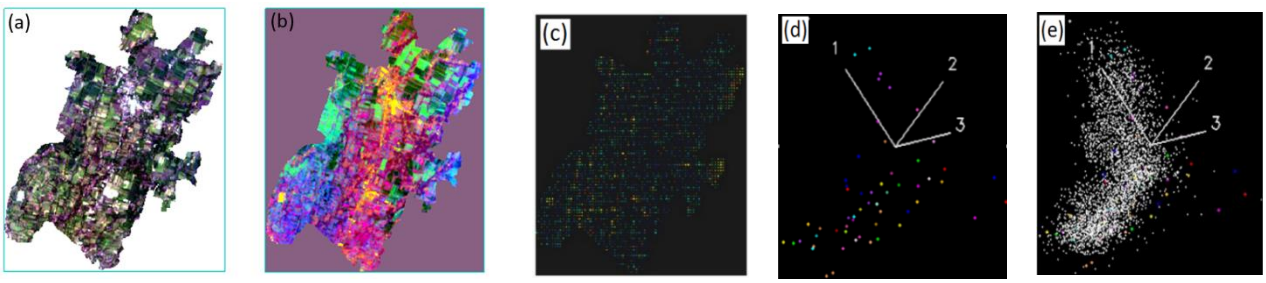

Figure 4: (a) Hyperspectral Reflectance Image; (b) Composite MNF Image; (c) PPI image result; (d) n-D visualizer 48 extreme pixel class; (e) pure pixel

Furthermore, MNF Eigenimages is used as input in the PPI process by using 5000 PPI iterations, and a threshold value of 2. PPI iteration process is shown in Figure 3c, where there are 872 pure pixels in early iteration and it continues to increase

until the iteration of 4200, the number of pure pixels is 4000 pixels. The output PPI pixel image that represents pure pixel is shown in Figure 4c. Furthermore, pure PPI pixel will be observed through the n-D visualizers, which shows the distribution of pure and extreme pixel that represents each class. Pure Pixel occurs around the extreme pixel edge. Through n-D visualizers, pure pixel can be selected and inserted into extreme class pixels. In the extreme pixel selection process, we must consider the majority of the selected pixel location. When it is away from the center and located near the other extreme, it is possible the pixel is not an extreme pixel. Further, it will produce a mixed pixel on endmember. Selection of a good pure pixel will consider the distance recorded as an extreme point of the center point and has a location close to the extreme edge corner pixel. The process of determining pure and extreme pixel is shown in Figure 4d and 4e.

The output generated through n-Dvisualizer for pure endmember is 48 endmember classes (Figure 5a), where there are 4 endmember classes: 1, 3, 6, 42 (non-vegetation) and 44 classes of vegetation. The paddy reflectance characteristic can be observed in the VIS-red edge region of value below 0.1. Vegetation endmember which has value below 0.1 are eliminated because the characteristic spectral curves do not meet the spectral curve of paddy. There are 12 classes of non-paddy vegetation, that is: 8, 12, 17, 20, 23, 26, 28, 32, 34, 40, 43, and 47. Thus, in a preliminary analysis, there are 32 endmember classes that are paddy endmember due to its characteristics meet the spectral curve of paddy (Figure 5b).

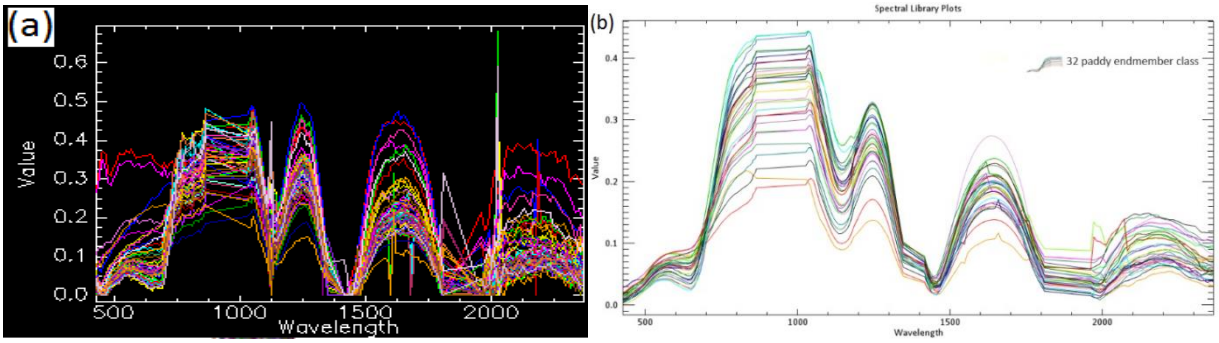

Figure 5: (a) 48 n-D visualizer Endmember Class; (b) 32 Class of Paddy Endmember reflectance.

Based on the paddy reflectance characteristics, the combination of characteristics of increasing/decreasing value in the VIS-red edge (447-701 nm), red edge-NIR (701-1027 nm) and NIR-SWIR (1027-1104 nm) range, may indicate the paddy growth stages, wherein the mean value in red edge-NIR can be used as predictors to distinguish planting stages. Based on these characteristics, the endmember can be divided into three categories. The first category is a curve that has increased value in the red edge-NIR (701-1027 nm) and NIR-SWIR (1027-1104 nm) range, in the value range of 0.2, and 0.3. The second category is a curve that has decreased red edge-NIR (701-1027 nm) range, but has increased value in the NIR-SWIR (1027-1104 nm), in the value range of 0.2<0.3, 0.3<0.4, and 0.4. The third category is a curve that has decreased value in red edge-NIR (701-1027 nm) and NIR-SWIR (1027-1104 nm) range, in the value range of 0.2<0.3 and 0.2<0.3. The classification category is shown in Table 3.

Table 3
Paddy Growth Stage Category

Red Edge - NIR	Value	NIR - SWIR	Endmember Class	Phase
Increase	0.2	Increase	21, 24	Week 6
	0.3		2, 35, 36, 39	Week 9
	0.4		4, 5, 29, 45	>Week 12
Decrease	0.3<0.4	Increase	25, 31	Week 15
	0.2<0.3		7, 9, 11, 18	>Week 15
Decrease	0.3-0.4	Decrease	10, 13, 14, 15, 16, 19, 22, 30, 33, 37, 38, 44, 46, 48,	Week 15
	0.2-0.3		27, 41	>Week 15

In the first category, the paddy reflectance has increasing value in the red edge-NIR and NIR-SWIR range. Reflectance can be categorized values range in red-edge and NIR. The reflectance value of 0.2 can be categorized as a phase of 6 weeks in the growth stage because the value of the VIS tends to be high (Figure 6a), while the value of 0.3, can be categorized as a phase of 9 weeks in the growth stage (Figure 6b).

In the second category, the curve has decreased value in red edge-NIR (701-1027 nm) but has increasing value in the NIR-SWIR (1027-1104 nm). Reflectance on the value of 0.4 can be categorized as phase planting on more than 12 weeks of the growth stage, because the value of the red edge-NIR (701-1027 nm) has begun to decrease, while the value of the NIR-SWIR (1027-1104 nm) still has increasing reflectance values (Figure 6c). At the 0.3 value <0.4, the reflectance can be categorized at the initial phase of 15 weeks in the growth stage beginning to show a decline, while the value of the NIR-SWIR (1027-1104 nm) still show an increase (Figure 6d). While in the 0.2 <0.3, reflectance can be categorized as phase planting more than 15 weeks, because the value of the red edge-NIR (701-1027 nm) began to show a decline, while the value of the NIR-SWIR (1027-1104 nm) still show an increase, while the value of the VIS will be a minimum (Figure 6e).

In the third category, the reflectance curve has decreased in red edge-NIR (701-1027 nm) and NIR-SWIR (1027-1104 nm), range in value of 0.3<0.4 and 0.2 <0.3. In value of 0.3<0.4, the reflectance can be categorized within a growth period of 15th week growth stage (Figure 6f), while the reflectance in the 0.2 <0.3 can be categorized as a phase of more than 15 weeks of the growth stage because of the value of red edge-NIR (701-1027 nm) diminishing to less than 0.3. (Figure 6g). The mean class of endmember reflectance based on each week growth stage are shown in Figure 6h. The further spectral unmixing process is done through SAM, to determined the paddy endmember. The pixel in the individual spectra image is compared with the pure pixel in the paddy growth stage spectral library endmember. Further, the similarity between the two spectra is determined by

establishing the rule and calculating the angle between the two spectra. The classification image generated trough SAM is illustrated in Figure 7.

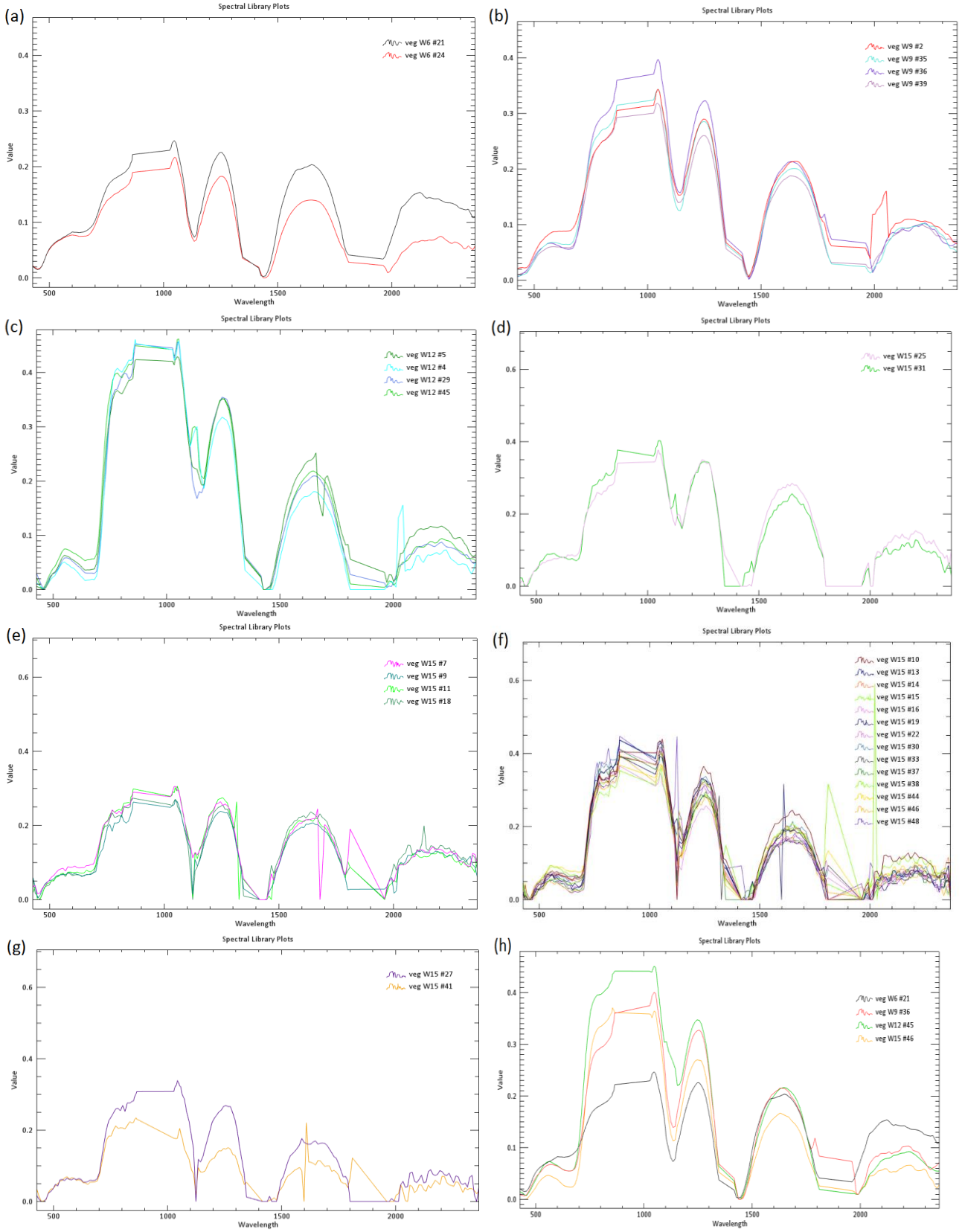

Figure 6: (a) reflectance endmember in 6th week;(b) reflectance endmember in 9th week; (c) reflectance endmember in 12th week; (d) Reflectance endmember of initial stage in 15th week within a range value of 0.3-0.4; (e) reflectance endmember of planting stage in 15th week within a range value of 0.2-0.3; (f) reflectance endmember in 15th week within a range value of 0.3-0.4; (g) reflectance endmember in week 15th week within a range value of 0.2-0.3; (h) and reflectance endmember mean class in 6th, 9th, 12th and 15th week.

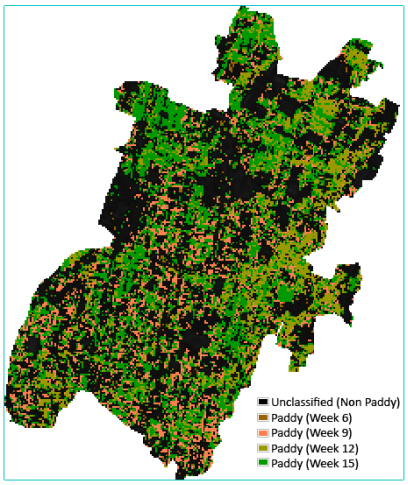

Figure 7: Paddy growth Stage Mapping using SAM

IV. DISCUSSION

In determining the new dimensionality with the MNF, the election threshold is important in determining the MNF band endmember. Considering too small threshold value (close to 1) will only produce a little number of endmember value while selecting a large threshold value, the MNF band will bring a lot of mixed pixels. Besides, the number of iterations and threshold in PPI is also very influential in producing pure pixels, which would later be pure pixel around the extreme pixel in n-D visualizers. In this study, a threshold value of 2 was selected in MNF and PPI process. Besides, 5000 iterations were used in PPI process. It produces 53 MNF band and 4000 pure pixels. Which later a number of 48 class of pure endmember extracted in the n-D visualizer process.

In this study, the wavebands that are sensitive to LAI and canopy content based on previous research used as a reference in build spectral library of paddy growth stage. Where the paddy wavelength reflectance optimal at wavelength 447, 701, 1024, and 1104 nm. Theses selected wavelength are used as the unique wavelength in each phase of VIS-red edge, red edge-NIR, and NIR-SWIR. In previous research, the selection of the VIS wavelength shows the absorption of chlorophyll and biomass content occur in green (519.559 nm) and Red (649 nm) [26], vegetation discrimination of paddy leaf photosynthetic pigments in the 426-671 nm [16], varied the wavelength 444, 554, 594, and 675 nm [23], 552 and 675 nm [22], as well as more generally in region of VIS-Red (350-1050 nm) [18]. Which in this study reflectance values in VIS-red edge region (447-701nm) with values <0.1, are used to distinguish paddy and non-paddy vegetation. In a previous study the transition between Red and NIR (red edge) has an important role in characterizing paddy reflectance based on the leaves chlorophyll content [24], varies at 700-750nm [16] [21], 705 and 776 nm [22], 729 nm [26][28], 723 [23], as well as more generally in region of VIS-SWIR 681-1104 nm [16]. In this study, these regions are used in determining the paddy growth stage based on the combination of the increase/decrease value in the region of edge red-NIR (701-1027 nm) and NIR-SWIR (1027-1104 nm), where the mean value of red edge-NIR used as predictors in distinguishing the growth stage. Besides, in a previous study the SWIR region used in determining variation in water content (1080-1170 nm) [16], also 1158, 1378 and 1965 nm [22]. In this study, the SWIR wavelength is used in determining the paddy growth stage at weeks 9 and 15, each of which is in the value of 0.3-0.4, wherein the 15th weeks the curve value will decrease, while in the 9th weeks of the curve value will increase. These determinations were based on previous studies of paddy reflectance characteristics during 3 weeks early planting, which influenced by soil and water content, while in 6th and 9th week phase the leaf area will increase, besides in 12th week the reflectance value of NIR will achieve the maximum value and achieve minimal value in VIS region [24].

V. CONCLUSION

PPI is a widely used in hyperspectral data processing because it can reduce dimensionality, and handle mixed pixel on large resolution images. Wavelength Selection in determining the optimal paddy vegetation occur in wavelength 447, 701, 1024, 1104 nm. In the region of VIS-red edge (447-701nm), curve below a value of 0.1 can be used to distinguish among paddy and non-paddy vegetation reflectance. Whereas in determining growth stage, it is based on the analysis of reflectance combination of the increase/decrease in the value of the edge red-NIR (701-1027 nm) and NIR-SWIR (1027-1104 nm), where the mean value in red edge-NIR can be used as predictors in distinguishing between the planting period and the mean value in the NIR-SWIR is useful in determining the growth stage at weeks 9 and 15, each of which are in 0.3-0.4 value. Which in week 15, the NIR-SWIR curve decreases, while in week 9, the curves still experience an increasing value. But the findings still need to be developed due to the possibility of information loss in endmember selection when deciding on the dimensionality of the data through the MNF, and the need for further research in modeling the characteristic curve based on paddy variety. Also, external factors can influence the paddy growth period of the spectral curve.

REFERENCES

[1] C. G. Karydas, "Temporal dimensions in rice crop spectral profiles," *Journal of Geomatics*, Vol 10 No. 2 October 2016, https://www.researchgate.net/publication/310524756

[2] B. M. Kumar, et al., "A Hybrid Classifier for Classification of Rice Crop Varieties, "*International Journal of Computer Science and Information Technologies (IJCSIT)*, Vol. 5 (2), 2014, 2224-2230, ISSN: 0975-9646

[3] Badan Penelitian dan Pengembangan Pertanian (Balitbangtan), "Varietas Padi Unggulan Badan Litbang Pertanian," *Agroinovasi Sinar Tani Badan Litbang Pertanian*, No.3441,25-31 Jan 2012. http://www.litbang.pertanian.go.id/download/one/355/varietaspadiunggulan.pdf

[4] Shwetank, J. Kamal, B. K. Jit, "Review of Rice Crop Identification and Classification using HyperSpectral Image Processing System," *International Journal of Computer Science & Communication IJCSS* Vol. 1, No. 1, January-June 2010, pp. 253-258.

[5] M. L. Gnyp, Y. Miao, F. Yuan, et al., "Hyperspectral canopy sensing of paddy rice aboveground biomass atdifferent growth stages," *Field Crops Research*, 155, 42–55, 2014, Elsevier, doi: 10.1016/j.fcr.2013.09.023

[6] D. Haldar, R. Nigam, C. Patnaik, et al., "Remote sensing-based assessment of impact of Phailin cyclone on rice in Odisha, India, "*Article in Paddy Water Environ*, The International Society of Paddy and Water Environment Engineering and Springer Japan, 2016, DOI 10.1007/s10333-015-0514-y

[7] USGS, *Earth Observing–1 (EO-1) Sensor Hyperion*, http://eo1.usgs.gov/sensors/hyperion

[8] J. B. Campbell, R. H. Wynne, *Introduction to Remote Sensing*. Fifth Edition. Guilford Press, 2013.

[9] P. Du, K. Tan, X. Xing, "A novel binary tree support vector machine for hyperspectral remote sensing image classification," *Optics Communications 285*, 2012. doi: 10.1016/j.optcom.2012.02.092

[10] R. George, H. Padalia, S. P. S. Kushwaha., "Forest tree species discrimination in western Himalaya using EO-1 Hyperion," *International Journal of Applied Earth Observation and Geoinformation 28*, 140–149, Elsevier, 2014. doi: 10.1016/j.jag.2013.11.011

[11] F. Utaminingrum, K. Uchimuraa, G. Koutakic, "Speedy filters for removing impulse noise based on an adaptive window observation," *International Journal of Electronics and Communications (AEÜ*), 95–100, Elsevier, 2014, doi: 10.1016/j.aeue.2014.07.017

[12] M. H. Mozaffar, M. J. V. Zoej, M. R. Sahebic, et. al., "Vegetation Endmember Extraction in Hyperion Images," *The International Archives of the Photogrammetry, Remote Sensing and Spatial Information Sciences*, Vol. XXXVII, Beijing, 2008.

[13] C. Zhang, "Multiscale quantification of urban composition from EO-1/Hyperion data using object-based spectral unmixing", *International Journal of Applied Earth Observation and Geoinformation*, 47, 153–162, Elsevier, 2016, doi: 10.1016/j.jag.2016.01.002

[14] R. A. Schwengerdt, *Remote Sensing: Models and Methods for Image Processing.*, 2nd. Ed., Academic Press, 1997, p.447.

[15] F. Chaudhry, S. Chakravarty, A. Plaza, et. al., "Design of Oast Algorithms for Pixel Purity Index for Endmember Extraction In Hyperspectral Imagery," *ASPRS 2005 Annual Conference Geospatial Goes Global: From Your Neighborhood to the Whole Planet*, Baltimore, Maryland, March 7-11, 2005.

[16] Shwetank, K. Jain, K. Bhatia, "Development of Digital Spectral Library and Supervised Classification of Rice Crop Varieties Using Hyperspectral Image Processing", *AARS*, 2011.

[17] X. Xiao, L. He, W. Salas, C. Li, B. Moore, R. Zhao, S. Frolking, S. Boles, "Quantitative relationships between field-measured leaf area index and vegetation index derived from vegetation images for paddy rice fields," *Int. J. Remote Sens*, 23(18):3595-3604, 2002. [doi: 10.1080/01431160110115799]

[18] P. S. Thenkabail, R. B. Smith, E. D. Pauw, "Hyperspectral vegetation indices and their relationships with agricultural crop characteristics," *Remote Sens. Environ*., 71(2):158-182, 2000. [doi:10.1016/S0034-4257(99)00067-X]

[19] P. S. Thenkabail, E. A. Enclona, M. S. Ashton, B. V. D. Meer, "Accuracy assessments of hyperspectral waveband performance for vegetation analysis applications", *Remote Sens. Environ*., 91(3-4):354-376,2004. [doi: 10.1016/j.rse.2004.03.013]

[20] C. Gonzalez, J. Resano, D. Mozos, et. al, "FPGA Implementation of the Pixel Purity Index Algorithm for Remotely Sensed Hyperspectral Image Analysis," *EURASIP Journal on Advances in Signal Processing, Volume 2010*, Article ID 969806, Hindawi Publishing Corporation, 2010. doi:10.1155/2010/969806

[21] C. Zhang, Z. Xie, "Combining object-based texture measures with a neural network for vegetation mapping in the Everglades from hyperspectral imagery," *Remote Sensing of Environment 124*, 310–320. Elsevier, 2012. doi: 10.1016/j.rse.2012.05.015

[22] S. Song, W. Gong, B. Zhu, et.al, "Wavelength Selection and Spectral Discrimination for Paddy Rice with Laboratory Measurements of Hyperspectral Leaf Reflectance," *ISPRS Journal of Photogrammetry and Remote Sensing*. 2011. doi: 10.1016/j.isprsjprs.2011.05.002

[23] F. M. Wang, J. F. Huang, X. Z. Wang, "Optimal waveband identification for estimation of leaf area index of paddy rice," *Journal of Zhejiang University*, SCIENCE B, ISSN 1862-1783 (Online), 2008.

[24] K. W. Chang, Y. Shen, J. C. Lo, "Predicting Rice Yield Using Canopy Reflectance Measured at Booting Stage," *Agronomy Journal*, 97: 872–8, 2005.

[25] C. Kuenzer, K. Knauer, "Remote sensing of rice crop areas", *International Journal of Remote Sensing*, Vol. 34, No. 6, 2101–2139, 20 March 2013. http://dx.doi.org/10.1080/01431161.2012.738946

[26] S. Moharana, S. Dutta, "Hyperspectral Remote Sensing of Paddy Crop Using In-Situ Measurement and Clustering Technique," *The International Archives of the Photogrammetry, Remote Sensing and Spatial Information Sciences*, Volume XL-8, ISPRS Technical Commission VIII Symposium, 09 – 12 December 2014, Hyderabad, India, 2014.

[27] C. H. T Daughtry, C. L. Walthall, M. S. Kim, E. B. de Colstoun, J. E. Mc-Murtrey, "Estimating corn leaf chlorophyll concentration from leaf and canopy reflectance," *Remote Sensing of Environment 74*, 2000 pp. 229-239.

[28] H. W. Jeffrey, Z. Chunhua, M. K. John, "Separating Crop Species in Northeastern Ontario Using Hyperspectral Data," *Remote Sens*., 6, 2014, pp. 925-945.

[29] S. Moharanaa, H. Medhib, S. Duttaa, "Advanced vegetation indices for sensing paddy growth via hyperspectral measurements," *Geocarto International*, ISSN: 1010-6049 (Print) 1752-0762 (Online), 2016, doi: 10.1080/10106049.2016.1232315

[30] P. Barry, *EO-1/Hyperion Science Data User's Guide,* Redondo Beach, CA: TRW Space, Defense & Informations Systems, 2001.

[31] B. Datt, et al. "Preprocessing EO-1 Hyperion hyperspectral data to support the application of agricultural indexes." *IEEE Transactions on Geoscience and Remote Sensing 41*, No. 6: 1246-1259, 2003.

[32] J. W. Boardman, F. A. Kruse, "Automated spectral analysis: a geological example using AVIRIS data, north Grapevine Mountains, Nevada,": in Proceedings, *ERIM Tenth Thematic Conference on Geologic Remote Sensing, Environmental Research Institute of Michigan*, Ann Arbor, MI, 1994, pp. I-407-I-418.

[33] F. Ramdani, "Urban Vegetation Mapping from Fused Hyperspectral Image and LiDAR Data with Application to Monitor Urban Tree Heights," *Journal of Geographic Information System*, 2013, 5, 404-408. doi:10.4236/jgis.2013.54038

[34] ENVI, *Advanced Hyperspectral Analysis*, ITT Visual Information Solutions.

[35] MicroImages Inc., *Pixel purity index and masking aid endmember selection*, TNTmips V6.10, 1999. http://www.microimages.com/documentation/TechGuides/61Ppi.pdf

[36] Harris Geospatial, *Pixel Purity Index Using ENVI*, http://www.harrisgeospatial.com/docs/PixelPurityIndex.html

[37] Harris Geospatial., *Spatial Data Reduction and Pixel Purity Index*., http://www.harrisgeospatial.com/Home/NewsUpdates/TabId/170/ArtMID/735/ArticleID/14288/Spatial-Data-Reduction-and-Pixel-Purity-Index.aspx

[38] J. W. Boardman, "Automating spectral unmixing of AVIRIS data using convex geometry concepts," In: *Summaries of the 4th Annual JPL Airborne Geoscience Workshop*, 1993, pp.11-14. ftp://popo.jpl.nasa.gov/ pub/docs/workshops/93_docs/4.PDF

[39] A. T. Harris, "Spectral mapping tools from the earth sciences applied to spectral microscopy data," *Cytometry*, 2006, pp.872-879. doi:10.1002/cyto.a.